Food Chemistry: X 18 (2023) 100692

Contents lists available at ScienceDirect

Food Chemistry: X

journal homepage: www.sciencedirect.com/journal/food-chemistry-x

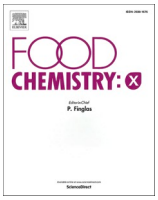

Novel iron-chelating peptide from egg yolk: Preparation, characterization, and iron transportation

Ying Liu [a], Zhuo Wang [a], Abulimiti Kelimu [b], Sameh A. Korma [c], Ilaria Cacciotti [d], Huan Xiang [a], Chun Cui [a,*]

[a] College of Food Science and Engineering, South China University of Technology, Wushan Road 381, 510640 Guangzhou, Guangdong, China
[b] College of Food Science and Pharmacy, Xinjiang Agricultural University, Nongda East Road 311, 830052 Urumqi, Xinjiang, China
[c] Department of Food Science, Faculty of Agriculture, Zagazig University, El-Zeraa Road 114, 44519 Zagazig, Sharkia, Egypt
[d] Department of Engineering, INSTM RU, University of Rome "Niccolò Cusano", 3 via Don Carlo Gnocchi, 3 00166 Roma, Italy

ARTICLE INFO

Keywords:
Egg yolk protein
Enzymatic hydrolysis
Iron chelate
Chelating mechanisms
Iron bioavailability

ABSTRACT

In this work, an egg yolk protein hydrolysate (EYPH) with a high iron-chelating ability (87.32%) was prepared. The fractionation using 60% (v/v) ethanol concentration (E3 fraction) led to the efficiently accumulating the iron-chelating peptides in EYPH. The characterization results showed that iron mainly chelated with carboxyl, amino and phosphate groups of peptides. From E3 fraction, six iron-chelating peptides with MW ranging from 1372.36 to 2937.04 Da were identified and a hypothesized molecular model of DDSSSpSpSpSpSVLSK-Fe was simulated. In vitro stability determination showed that E3-Fe chelate owned a good heat, alkalinity and digestion tolerance, but a relatively bad acid tolerance. Finally, iron transport analysis showed that iron in the E3-Fe would be absorbed in caco-2 cell membrane more effectively than that of iron salts, indicating that it was possible to apply the E3-Fe complex as iron supplements.

1. Introduction

Iron, as an indispensable component of cytochrome, enzymes, haemoglobin and myoglobin, plays a critical role in regulating many vital physiological processes such as oxygen transport, electron transfer reactions, gene regulation and cell growth, and differentiation via a series of mechanisms (Sophie et al., 2014). Iron deficiency, which is the result of insufficient dietary intake or poor utilization of iron, is the most common nutritional disorder. Nowadays, it is considered a global public health problem as it is a leading risk factor for anaemia, cancer, poor cognitive development, and even maternal mortality. Even though dietary iron can be obtained from a wide variety of animal and plant-sourced foods, the dietary intake of iron is limited due to its low bioavailability (Steinbicker & Muckenthaler, 2013).

More recently, various iron supplements have been developed such as including inorganic salts, organic acid salts and metal agents. However, traditional salt-based fortification methods have some limitations due to their deleterious effects on food's physical and sensory properties. Besides, iron salts have side effects on the consumer's health upon administration (Zhang et al., 2021). In this context, iron chelating peptides, owing to their superiority in terms of bioavailability, absorption rate, and stability, are increasingly attracting the scientific community attention (Abdul et al., 2022). During the past decades, many studies have addressed the role of iron-chelating peptides from several sources including *Acetes japonicas*, mung bean, whey protein, rice bran, vegetable protein, etc (Kong et al., 2021). The related research results indicated that the type of the used enzyme, protein source and hydrolysis conditions influence the iron-chelating ability of hydrolysate (Wu et al., 2021). Moreover, it has also been reported that the net charge, side chain length and functional groups of the amino acids also play a crucial role in the iron-chelating ability of peptides, including specific phosphate groups of serine, carboxyl groups of glutamic acid and aspartic acid, guanidine of arginine and amino group of lysine (Shi et al., 2021; Sun et al., 2017). Despite there are some results assuming that the above-mentioned factors are possibly related to the iron-chelating ability of peptides, its mechanism was much more complicated and still far from being entirely understood.

Egg yolk is one of the most readily available and widely consumed food in the human daily diet and consists of a wide spectrum of nutrients (lipids, proteins, vitamins, and metal ions) that are needed for cell and

* Corresponding author.
E-mail address: cuichun@scut.edu.cn (C. Cui).

https://doi.org/10.1016/j.fochx.2023.100692
Received 31 January 2023; Received in revised form 9 April 2023; Accepted 21 April 2023
Available online 22 April 2023

tissue development, function and survival (Guilmineau et al., 2005). Particularly, egg yolk protein is a novel high-quality protein with high biological value. Egg yolk is mainly composed of γ-livetin and phosvitin which were reported to have varieties of physiological activities such as immune, antioxidant, promoting bone growth, bacteriostatic, blood pressure lowering and metal ions binding activities (Aluko & Mine, 1997; Huang & Ahn, 2019; Shi et al., 2021; Zambrowicz et al., 2012). In contrast to egg white, egg yolk has a high proportion of lipids. Therefore, egg yolk has long been used in the food and cosmetics industry to produce lecithin (Peñaranda-López et al., 2020). The remaining defatted egg yolk powder (DEYP) after lecithin extraction, however, has low functionality due to its partial denaturation during the extraction, thus limiting its application and causing a waste of protein resources. Therefore, further studies should be required to increase the economic value of DEYP.

In light of the above considerations, the objective of this study was to obtain high iron-chelating peptides from DEYP by enzymatic and ethanol precipitation technology. Molecular weight (MW) distribution, hydrophobicity and amino acid composition, Fourier transform infrared (FTIR) spectroscopy, differential scanning calorimetry (DSC), and mass spectrometry were used to clarify the binding mechanism between egg yolk peptides and iron. Finally, the *in vitro* stability and iron transport analysis of iron-peptides chelate were investigated to evaluate its potential as an iron supplement.

2. Materials and methods

2.1. Materials and chemicals

Defatted egg yolk powder (DEYP) was obtained from Guangzhou Yingzhu Biological Technology Co., Ltd (Guangzhou, China). Alkaline protease was purchased from Novozymes Company (Tianjin, China). The reagents used in the high-performance liquid chromatography (HPLC) and liquid chromatography-mass spectrometry (LC-MS/MS) experiment were offered by Beijing Solarbio Science & Technology Co., Ltd (Beijing, China). All other reagents were of analytical grade and purchased from Fuchen Chemical Reagent Co., Ltd (Tianjin, China).

2.2. Determination of the proximate composition

A proximate analysis (moisture, ash, fat and protein contents) of the DEYP was carried out using the method described by AOAC (AOAC, 1995). The total sugar content was assessed with the phenol–sulphuric acid method described by The People's Republic of China (GB/T 15038–2006). All measurements were performed in triplicate and the absolute difference between the two independent measurements did not exceed 5% of the arithmetic mean.

2.3. Preparation of egg yolk protein hydrolysates (EYPH)

The effects of solution pH (6, 7, 8, 9, 10 and 11), enzyme concentrations (0.20, 0.60, 1.00, 1.40 and 1.80 %), hydrolysis temperatures (35, 45, 55, 65 and 75 °C) and hydrolysis times (0, 3, 6, 9, 12 and 24 h) on iron-chelating ability assays were studied by single factor design. Prior to the hydrolysis, the DEYP was smashed by pulverizer and passed through an 80 meshes sieve. Then, the powdered sample was dispersed in distilled water at a 1:9 (w/v) ratio and the solution pH was adjusted with 1 mol/L NaOH. Afterwards, the hydrolysis reaction was started by the alkaline protease addition. At the end of the reaction, the enzyme was inactivated by heating the hydrolysate at 100 °C for 15 min. Subsequently, the mixture was centrifuged (8000 × g for 15 min) and the supernatant was separated and lyophilized for further use. On the basis of the single-factor experiment results, the mathematical regression model for optimizing the hydrolysis process was established by means of the response surface methodology.

2.4. Determination of the metal ion-chelating activity

The iron-chelating activity of EYPH was measured according to the method of a previous study with slight modifications (Torres-Fuentes et al., 2012). Briefly, the EYPH sample (1 mL, 1.0 mg/mL) was mixed with 3.7 mL of 0.05 mol/L sodium acetate buffer (pH = 5) and 0.1 mL of 2 mmol/L $FeCl_2$ solution (water was used as a control). After incubation at room temperature for 10 min, the binding reaction of the mixture was terminated by adding 0.2 mL of 5 mmol/L phenanthroline into the solution. The absorbance of the obtained complex was measured at 562 nm after 10 min. The formula for iron-chelating ability was as follows:

$$\text{Chelating rate}\,(\%) = \frac{A_{total} - (A_{sample} - A_{blank})}{A_{total}} \times 100$$

where A_{total}, A_{sample} and A_{blank} represent the absorbance values of the total mixture, the sample and the blank, respectively.

The calcium and copper chelating activity of EYPH was determined using the EDTA titration method. Briefly, EYPHs were transferred into a new glass tube, and the pH was adjusted to 7.0 with a solution of NaOH (1 mol/L) before the addition of $CaCl_2$ or $CuSO_4$ solution. The resulting mixture was subjected to stirring at 37 °C for 40 min. The Ca^{2+} or Cu^{2+} content in the supernatant was evaluated using the ethylenediaminetetraacetic acid (EDTA) method.

2.5. Determination of the degree of hydrolysis (DH)

The ammonia nitrogen (AN) content was determined by the formol titration method (Xie et al., 2021). Briefly, EYPH solutions (5 g) were mixed with distilled water (75 g) and the pH was adjusted to 8.2 with 0.1 mol/L NaOH. Then 10 mL of 38% (v/v) formaldehyde solution was added and the total mixture was left at the room temperature for 5 min. The mixture was then titrated with 0.1 mol/L NaOH until a pH of 9.2. The distilled water was taken as the blank. The total nitrogen (TN) in the sample was determined by the Kjeldahl method. The content of the AN and the DH was calculated as follows:

$$\text{AN}\,(\%) = \frac{(V1 - V0)*C*0.014*100}{m}*100$$

$$\text{DH}\,(\%) = \frac{AN\ content\ in\ supernatant}{TN\ content\ in\ raw\ materials}*100$$

where V_1 and V_0 are the volumes of NaOH used for the titration of the sample solutions and water (blank experiment), respectively, C is the concentration of NaOH and m is the amount (g) of the sample solutions (Zhao et al., 2018).

2.6. Isolation and purification of egg yolk peptides (EYP)

Based on the ethanol precipitation method, EYPH was subjected to stepwise fractionation into four different fractions using elevated concentrations (20, 40, and 60%, v/v) of aqueous ethanol solutions. Firstly, the fractionation of EYPH was induced by adding anhydrous ethanol into the EYPH solutions (25%, w/v) to a final ethanol concentration of 20% (v/v). The mixture was held for 1 h and centrifuged at 9000 × g for 20 min and the precipitate was labelled E1. Secondly, the ethanol concentration of 40% and 60% was used to separate the EYPH, all steps were similar to the first step except for the ethanol concentration. The precipitate obtained successively was labelled E2 and E3, and the final supernatant was labeled E4, respectively. All fractions were freeze-dried for later use.

2.7. Molecular weight (MW) analysis

The MW distribution was determined using high-performance liquid chromatography (HPLC, Agilent 1200LC, USA), according to Chang et al

(Chang et al., 2021). Prior to the chromatographic analysis, the samples were dissolved in deionized water to a 10 mg/mL protein concentration and filtered through a 0.45 μm filter. Samples (20 μL) were loaded into the sample loop, using a microliter syringe, and separated by the TSK-GEL G2000SWXL size exclusion column (Tosoh Bioscience, Tokyo, Japan). For the EYPH fractions separation, a flow rate of 0.5 mL/min of acetonitrile in isocratic mode at 37 °C was used and the detection wavelength was 220 nm. A mixture of standards was used to cover the range of 100–70000 Da, as follows: bovine serum albumin, 68000 Da; cytochrome *C*, 12384 Da; aprotinin, 6511 Da; bacitracin, 1423 Da; glutathione, 189 Da. Finally, the relative molecular mass calibration curve was drawn, with the retention time as the abscissa and the logarithm of the relative molecular mass as the ordinate MW distribution was calculated.

2.8. Analysis of amino acid composition

The amino acid composition and content were analyzed according to the method reported by Liu et al (Liu et al., 2018). The samples were subjected to acid hydrolysis with 6 M HCl at 110 °C for 24 h. The hydrolyzate was vacuum dried until waterless, mixed with sodium citrate buffer and analyzed by an amino acid analyzer (HITACHI L-8900, Japan).

2.9. Peptide identification by LC-MS/MS

The freeze-dried E3 fraction was dissolved in deionized water to a 0.1% (v/v) solution, desalted and concentrated onto OMIX pipette tips C18. The column information is: 300 μm × 5 mm, Acclaim PepMap, RSLC C18, 5 μm (Thermo, 160454); Acclaim PepMap 75 μm × 150 mm, C18, 3 μm (Thermo, 160321). The mobile phase was: solvent A: water (0.1% (v/v) formic acid); solvent B: acetonitrile (0.1% (v/v) formic acid); flow rate: 300 μL/min. The gradient profile was set as follows: 0–5% solvent B for 5 min, 5–45% solvent B for 40 min, 50–90% solvent B for 5 min, 90% solvent B for 5 min and 90–5% solvent B for 5 min. The separated peptides were split through the spray voltage and detected by electron spray ionization in survey scans from 100 to 2000 *m/z*. Later, high-purity nitrogen (98%) was used as atomizing and drying gas, the drying temperature was 180 °C, and the drying gas flow rate was 4.0 L/min. The original data was converted by MM File Conversion, and the Uniprot database was searched by MASCOT to obtain the target polypeptide sequence. The identification of the phosphorylation site was according to the specific increasing value (+79.996) of the mass-to-charge ratio (*m/z*) of peptides. The relative content of the peptide was calculated by the ionic strength of the peptide.

2.10. Fourier transform infrared (FTIR) spectroscopy

The E3 and E3-Fe chelate complexes were characterized by an Infrared spectrophotometer (IS50, Thermo Nicolet Corporation, Wisconsin, USA) using the KBr compression method (Fang et al., 2020). 0.5 g of E3 and E3-Fe^{2+} chelate freeze-dried powders were weighed, added with potassium bromide, evenly mixed, ground and pressed to obtain a tablet, and scanned in the wavenumber range of 400–4000 cm^{-1}. The spectrum obtained was analyzed by Ominic software, and the secondary structure was analyzed by Peakfit 4.0 software.

2.11. Differential scanning calorimetry (DSC)

DSC thermograms of E3 and E3-Fe^{2+} chelate complexes were recorded using a differential scanning calorimeter (PEAQ-DSC MicroCal, Northampton, MA, USA) to evaluate the thermal properties (Cai et al., 2019). An appropriate amount (3 mg) of E3 and E3-$Fe2^{+}$ chelate freeze-dried powders were weighed in the crucible and placed in the instrument for thermal stability analysis. The parameters were as follows: temperature range of 25–200 °C, the heating rate of 10 °C /min and the N_2 flow rate of 50 mL/min.

2.12. In vitro stability of E3-Fe chelate

For acid-base tolerance studies, E3-Fe sample was mixed with water (1%, m/v) at seven different pH (3, 4, 5, 6, 7, 8, 9 and 10) values. For high-temperature tolerance studies, E3-Fe sample was mixed with water (1%, m/v) and placed in the shaking water bath at different temperatures (30, 40, 50, 60, 70 and 80 °C). All tolerance tests lasted for 1 h, the free iron release was used to evaluate the stability. The digestion stability of the E3-Fe was referred to the method described by Zhang et al. (Zhang et al., 2021). The prepared E3-Fe (0.1 g) was dissolved in 100 mL water, gastric digestion was conducted using pepsin (5 mg/mL) at pH 2 (adjusted with 1 M of HCl) under 37 °C. The digestive system was incubated for 2 h and neutralized with NaOH (1 M). Then, the intestinal digestion was carried out using trypsin (2 mg/mL at pH 7 under 37 °C for 4 h) using an air shaker. After the process was completed, sodium carbonate was added to quench the reaction. The supernatant was collected after centrifugation (10000 × g, 10 min) and the free iron content was determined using the phenanthroline colorimetry method. The digestion stability of the E3-Fe was evaluated by the free iron increase in the supernatant.

2.13. Iron transport studies in Caco-2 membrane

Cytotoxicity experiments were performed using MTT (3-[4,5-dimethylthiazol-2-yl]-2,5 diphenyl tetrazolium bromide) kit before iron transport studies. In the iron transport experiment, Caco-2 cells were employed as a model of the intestinal epithelium (Jantarajit et al., 2007). Caco-2 cells (1 mL) were seeded on 12-well polyester transwell inserts (0.4 μm pore size, 12 mm diameter, corning) with a cell density of 1×10^5 cells/mL and 21 days incubation. The culture medium was daily changed after 24 h of seeding and the volume of the culture medium was 0.5 mL and 1.5 mL on the apical side (AP) and basolateral side (BL), respectively. During the 21-day incubation, transepithelial electrical resistance (TEER), alkaline phosphatase activity ratio (ALP, AP/BL), and sodium fluorescein permeability (SFP) were monitored. The Caco-2 cell monolayers were used for the calcium transport experiments until the TEER, ALP and SFP reached 400 Ω × cm^2, 31.60 and 41.43%, respectively. After cell wells were washed twice with PBS (pH 7.4), 1 mL of $FeSO_4$ (55, 110 and 220 μg) and E3-Fe (0.5, 1 and 2 mg/mL; 40 Fe μg/mg) were added to the AP side, separately. Transwell plates were incubated in an incubator (37 °C, 5% CO_2) for 4 h, and 1 mL solution was collected from the BL to measure the ferrous iron concentration by using flame atomic absorption spectroscopy. Three replicates were performed for each group.

2.14. Statistical analysis

Statistical analysis was carried out with SPSS (version 16.0). For significant main effects, means were considered to be different at a significance level of 0.05. Data were expressed as means of three replicates.

3. Results and discussion

3.1. Proximate composition of defatted egg yolk powder (DEYP)

DEYP, the by-product after the egg yolk lecithin extraction, is rich in proteins and owns various biological activities. The proximate composition of DEYP was determined. As expected, DEYP showed a high amount of proteins (79.88 ± 0.23%) and a small quantity of fat (5.08 ± 0.74%), ash (4.78 ± 1.26%, including iron 2.70 mg/100 g), water (4.36 ± 0.31%) and sugar (0.2 ± 0.09%).

3.2. Choice of chelated metal ions

The egg yolk protein hydrolysate (EYPH) generated during the hydrolysis with the alkaline protease may possess different chelating ability towards different metal ions, such as iron, calcium and copper. To test this hypothesis, preliminary experiments on the EYPH chelating ability towards these divalent metal ions were conducted under the same operative conditions and results were compared with those of casein phosphopeptide (CPP). Fig. S1 shows that the metal ions-chelating ability significantly increased with the hydrolysis time during the first 3 h and started to decrease afterwards. EYPH exhibited the highest iron-chelating ability, followed by calcium and copper. As compared to CPP, the EYPH chelating ability towards calcium and copper was lower, while the iron-chelating ability was significantly higher even at lower protein concentrations than the control group. Therefore, it can be concluded that the iron-chelating ability of EYPH is competitive compared with calcium and copper. The differences in the metal-chelating ability observed for the EYPH could be attributed to chemical and physical differences between these metal ions and the peptide structure (Dudev & Lim, 2014).

3.3. Optimization of the enzymatic hydrolysis process

Single-factor experiments were used to investigate the effects of hydrolysis parameters, including the enzyme concentration, temperature, pH and hydrolysis time, on the DH and iron-chelating ability of the EYPH. The DH is an important indicator of the enzymatic hydrolysis, as it is directly related to the hydrolyzate functionality (Nisov et al., 2020). As shown in Fig. 1A, the DH showed a significant increase as the enzyme concentration increased from 0.2 to 1.8%. Accordingly, the increase in the enzyme concentration from 0.2 to 1.0% led to the increase in the iron-chelating ability: the EYPH with a DH of 14.77% showed the highest iron-chelating ability (86.37%) at 1.0% of the enzyme concentration. However, further increasing the enzyme concentration from 1.0 to 1.8% resulted in a decrease in the iron-chelating ability, indicating that a lower or higher enzyme concentration might lead to inadequate or excessive substrate hydrolysis, respectively, thereby affecting the iron-chelating ability (Vo et al., 2020). Based on the reported results, it could be suggested that, to some extent, the DH is not directly linked to the iron-chelating ability of EYPH, where appropriate hydrolysis is crucial for obtaining a hydrolyzate with high iron-chelating ability (Budseekoad et al., 2018). The iron-chelating abilities of EYPH obtained after different hydrolysis times were investigated and the related results are shown in Fig. 1B. A significant increase in the DH and iron-chelating ability was observed during the first 3 h: the EYPH with a DH of 14.77% possessed the highest iron-chelating ability (87.61%) at 3 h, after which a gradual decline was observed for the iron-chelating ability, while the DH gradually increased afterwards. These results are in agreement with the observations of another study (Sun et al., 2017). This variation in the DH and iron-chelating ability of the EYPH over time might be due to the continuous formation and degradation of the iron-binding peptides by an increased hydrolyzing effect of the alkaline protease (Hernández-Ledesma et al., 2002). The temperature is one of the most important parameters in the enzymatic hydrolysis as it leads to the substrate and enzyme conformational changes, metal–ligand interaction and kinetic energy of enzymatic reactions (Sun et al., 2001). The temperature effect on the DH and iron-chelating ability was studied by using a temperature ranging from 35 to 70 °C. Fig. 1C shows that the DH and iron-chelating ability significantly increased by raising the temperature from 35 to 55 °C, reaching the maximum of 15.01 and 84.67% at 55 °C, respectively. However, the DH and iron-chelating ability decreased as the temperature increased from 55 to 70 °C, indicating that the high temperature might lead to a permanent loss of the enzyme activity due to the enzyme denaturation (Thiansilakul et al., 2007). As shown in 1D, the pH significantly influenced the DH and iron-chelating ability of EYPH. The increase in the reaction pH from 7 to 11 caused an increased trend of the DH and iron-chelating ability, which reached the highest value (15.27 and 90.78%, respectively) at pH 11. The increased DH value with

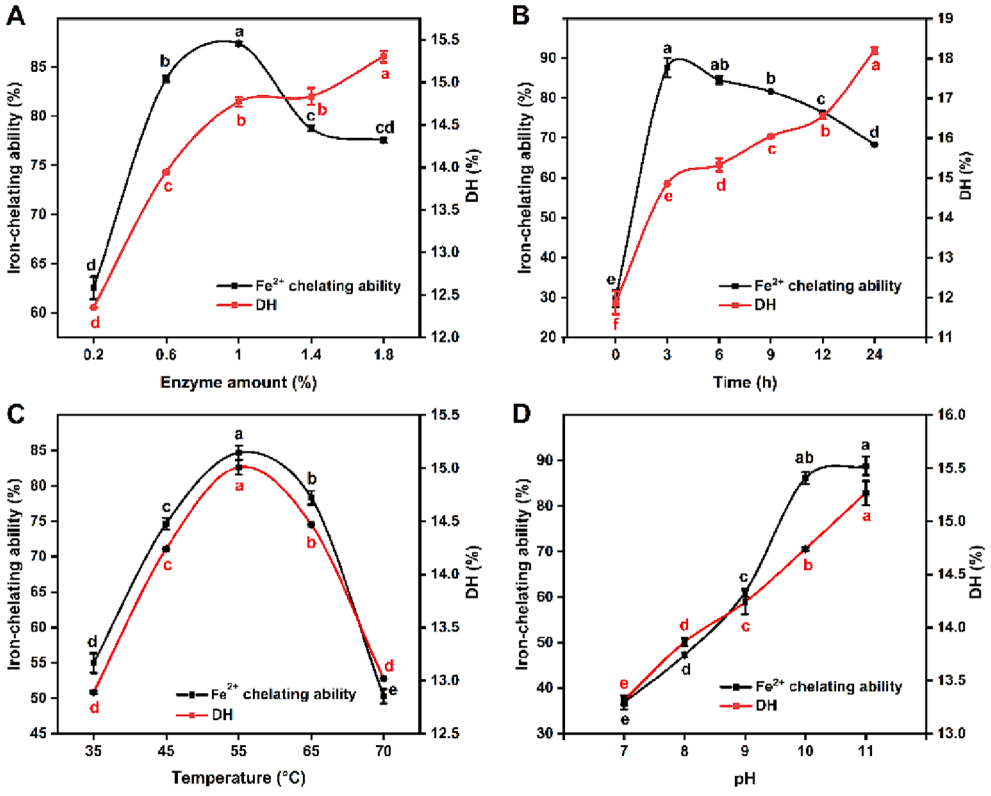

Fig. 1. Effect of the enzyme amount, time, temperature and pH on the iron-chelating ability and DH: (A) enzyme amount; (B) enzymatic hydrolysis time; (C) Eenzymatic hydrolysis temperature; (D) enzymatic hydrolysis pH.

increasing pH could be due to the disruption of phospho-calcic bridges between high-density lipoproteins and phosvitin compact complexes under the condition of charge distribution change. Besides, the substrate and enzyme conformation resulted in an increased solubility of the egg yolk proteins and thus a substrate was able to interact with the enzyme more easily. Moreover, the egg yolk protein isoelectric point ranged between 5 and 6, and the pH increase leads to a negative charge increase, resulting in the exposure of more –COO- groups and high iron-chelating activity of EYPH (Huang et al., 2021; Thiansilakul et al., 2007).

Based on the results of the single-factor experiments, different independent variables were selected to study their effect on the EYPH iron-chelating ability using the response surface methodology. The results of 17 experiments with different conditions are shown in Table S1 and the iron-chelating ability of EYPH ranged from 64.12 to 87.53%. It can be seen from Table S2 that the p value (0.0001) of the model is extremely significant ($p < 0.01$), the determination coefficient ($R^2 = 0.9913$) and the adjusted determination coefficient ($R^2_{adj} = 0.9802$) are quite close, indicating that the regression model is well fitted. The optimal hydrolysis conditions obtained by the quadratic experiment model are as follows: hydrolysis time 3.22 h, hydrolysis temperature 55.59 °C, enzyme concentration 1.08%. Under the predicted optimal conditions, the theoretical iron-chelating ability of EYPH was 88.57%.

3.4. Total nitrogen (TN) and iron-chelating ability determination

The fractionation of the EYPH into distinct fractions might help enrich some fractions with higher bioactivity as compared to the original mixture. The gradient ethanol precipitation was used for separation in this objective and the EYPH was separated into four different fractions (E1, E2, E3, and E4) with gradient ethanol concentrations (20, 40 and 60%). Fig. 2 shows the TN and iron-chelating ability of different fractions obtained by the ethanol fractionation. The TN content of the E1 was the highest and gradually decreased until E3 fraction. Interestingly, although characterized by the lowest TN content, the E3 fraction exhibited the highest iron-binding ability, which was significantly higher than that of other samples. This might be mainly attributed to the dual effects of the ethanol precipitation as enrichment of the target peptides and reduction of peptides interactions by removing non-similar peptides, which was likely to improve the iron-chelating ability of fractions further (Caetano-Silva et al., 2015).

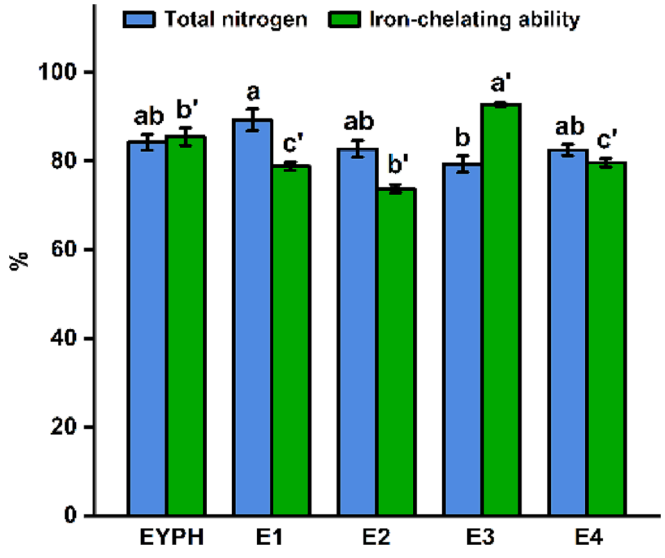

Fig. 2. Total nitrogen and iron-chelating ability of different components obtained by the ethanol fractionation.

3.5. Surface hydrophobicity analysis

The surface hydrophobicity refers to the hydrophobic amino acids distribution on the proteins/peptides surface by structural changes, which is related to the functional properties of the proteins or hydrolyzate (Liu et al., 2015; Liu et al., 2010). The surface hydrophobicity of the different fractions obtained by the ethanol fractionation is shown in Fig. 3A. Different fractions showed significantly different surface hydrophobicity. The fractions surface hydrophobicity progressively increased with increasing the ethanol concentration from 20 to 60% with the fraction E3 showing the highest value, while the lowest surface hydrophobicity was observed for supernatant (E4). The hydrolyzate hydrophobicity depends on the substrate nature and the peptides MW (Calderón de la Barca et al., 2000). It is well known that the ethanol dielectric constant is lower than that of the water. In the EYPH system, the dielectric constant of the solution decreased with the increase of the ethanol volume fraction, the ethanol molecules diffused to the peptide surface, bound to the hydrophobic region and resulted in the precipitation. At the same time, the hydrophobic region buried inside the protein was gradually exposed to the surface, which destroyed the peptide's natural structure and led to the high hydrophobicity (Shi et al., 2015). The exposing hydrophobic groups might provide more sites that bind to the iron, and it might be the reason why the E3 component had a high iron-chelation rate (Mattar et al., 2022).

3.6. Molecular weight (MW) distribution analysis

The alkaline protease, with its broad specificity and preference for hydrophobic residues, represents a good candidate for producing low free amino acids in the hydrolyzate as compared to other proteinases. The ethanol fractionation with increasing concentration from 20 to 60% (v/v) led to a gradual change in the percentage of MW distribution in the different fractions, confirming the occurrence of the ethanol-induced aggregation. As shown in Fig. 3B, the lowest percentage of high MW (greater than5000 Da) fragments was observed in E4, and the percentage of this fragment gradually decreased from 9.73% (EYPH) to 5.21% (E4) with the fractionation. The percentage of 1000–5000 Da fragments gradually increased for fractions E1 (24.79%), E2 (29.87%) and E3 (33.45%), but for E4 (20.40%) a significant decrease was observed. As for the percentage of smaller MW fragments (<1000 Da), a gradual decrease from fractions E1 to E3 (69.63–61.55%) was revealed, whereas a significant increase was evidenced for E4 (74.28%), indicating that the ethanol addition up to a certain concentration could lead to a pronounced variation in the composition between the precipitate and supernatant.

3.7. Amino acids composition

The iron-chelating activity of different fractions can be attributed to the composition and sequences of amino acids (Torres-Fuentes et al., 2012). On the basis of the high iron-chelating ability of the E3 fraction, it is supposed that the gradient ethanol precipitation process might enrich the peptides with specific amino acids with high chelating ability. Herein, the composition and content of amino acids in EYPH and fractions with the highest iron-chelating activity (E3) were further analyzed. As shown in Table 1, a total of 17 different amino acids, including 9 hydrophilic and 8 hydrophobic amino acids, in both EYPH and E3 was determined. The results evidenced that EYPH and E3 had similar amino acids composition, but significantly ($P < 0.05$) differed in some amino acids content. The amino acids profile of EYPH showed that glutamic acid was the most abundant amino acid (14.50 g/100 g), followed by aspartic (10.72 g/100 g), leucine (8.62 g/100 g), lysine (7.54 g/100 g) and serine (7.36 g/100 g), relative to other amino acids. In contrast, the major amino acids in the E3 fraction were glutamic (12.90 g/100 g), serine (12.47 g/100 g), aspartic (10.67 g/100 g), lysine (9.63 g/100 g) and arginine (8.83 g/100 g). Besides, the serine and lysine content in E3

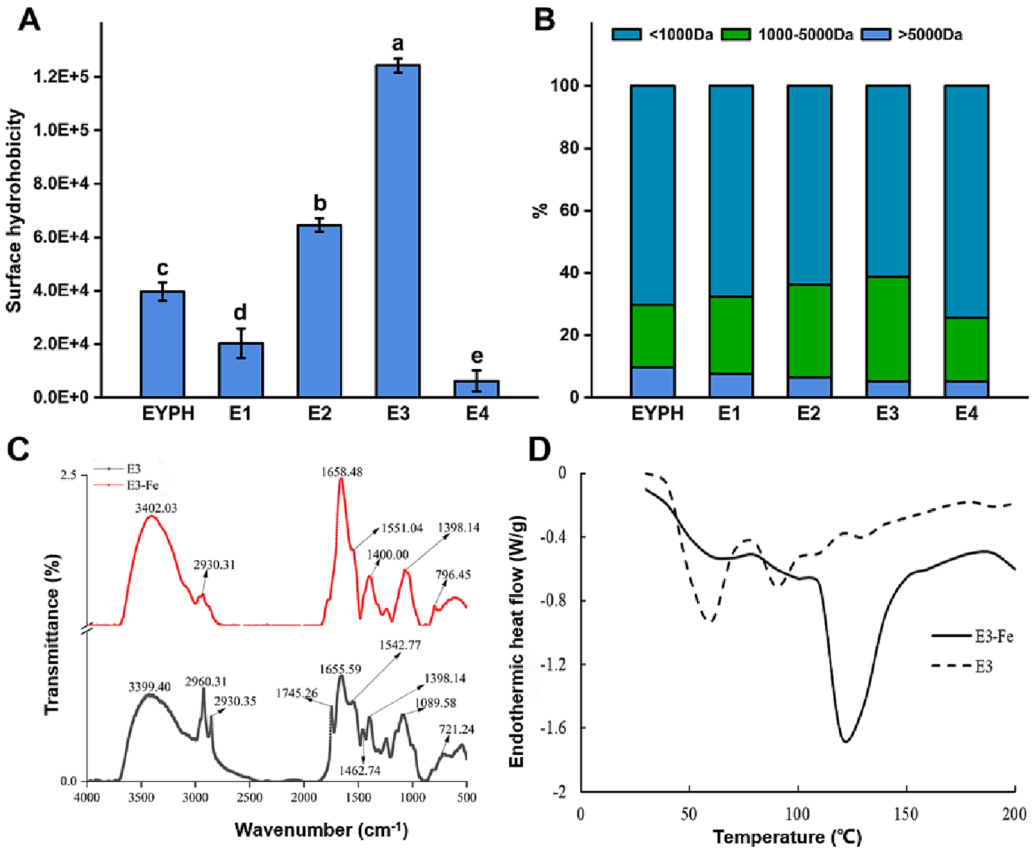

Fig. 3. Structure analysis of different components (E1, E2, E3 and E4) obtained by the ethanol fractionation and the E3-Fe chelate: (A) surface hydrophobicity of different components btained by the ethanol fractionation; (B) molecular weight distribution of different components btained by the ethanol fractionation; (C) Fourier Transform infrared spectra of E3 and E3-Fe; (D) differential scanning calorimetry (DSC) thermograms of E3 and E3-Fe.

Table 1
Amino Acid Composition of Egg Yolk Protein Hydrolysate (EYPH) and E3 Component.

Amino acid	EYPH	E3	*P*-value
aspartic acid	10.72 ± 0.11	10.67 ± 0.09	0.759
threonine	5.80 ± 0.01^{a}	5.53 ± 0.02^{b}	0.007
serine	7.36 ± 0.21^{b}	12.47 ± 0.19^{a}	0.003
glutamic acid	14.50 ± 0.23	12.90 ± 0.41	0.077
glycine	3.64 ± 0.09^{a}	3.22 ± 0.03^{b}	0.047
alanine	5.64 ± 0.01^{a}	4.94 ± 0.02^{b}	0.001
cystine	1.05 ± 0.00^{b}	1.13 ± 0.01^{a}	0.015
valine	6.64 ± 0.11^{a}	4.76 ± 0.08^{b}	0.005
methionine	2.48 ± 0.08^{a}	1.72 ± 0.03^{b}	0.012
isoleucine	4.61 ± 0.23	3.79 ± 0.17	0.103
leucine	8.62 ± 0.30	6.22 ± 0.59	0.068
tyrosine	4.35 ± 0.01^{a}	3.50 ± 0.07^{b}	0.007
phenylalanine	4.51 ± 0.02^{a}	3.95 ± 0.09^{b}	0.026
lysine	7.54 ± 0.09^{b}	9.63 ± 0.15^{a}	0.007
histidine	2.28 ± 0.01^{b}	2.83 ± 0.04^{a}	0.006
arginine	6.34 ± 0.10^{b}	8.83 ± 0.10^{a}	0.003
proline	3.92 ± 0.06	3.90 ± 0.10	0.880
Hydrophobic amino acid	40.06 ± 0.11^{a}	32.50 ± 0.21^{b}	0.001
Hydrophobic Q value	4.36 ± 0.09	3.82 ± 0.10	0.057

Means in the same line followed by the different letter are significantly different ($p < 0.05$).

was significantly higher that that of EYPH. Many studies have found that histidine, glutamic acid, aspartic acid, and lysine are amino acids related to the chelation of ferrous ions which can provide binding site for ferrous ions. In addition, phosphoserine residues have also been identified as important amino acids associated with iron binding (O'Loughlin et al., 2015). Therefore, it appears that the ethanol fractionation leads to the enrichment of serine and lysine containing peptides, thereby exhibiting high iron-chelating activity.

3.8. Fourier transform infrared (FTIR) spectroscopy and differential scanning calorimetry (DSC)

In order to unravel the precise iron binding sites of the peptides, the FTIR spectroscopy was employed to examine the shift of characteristic absorption peaks. Indeed, the variation in the absorption peaks of the FTIR spectra could reflect the interaction of metal ions with organic ligand groups in the peptides. As illustrated in Fig. 3C, several characteristic absorption peaks of E3 shifted upon the coordination with irons. The coordination with irons led to the E3 absorption peak shift from 3431.40 to 3402.03 cm^{-1}, suggesting an involvement of the *N*-terminal amino group and the amino group in the side chains (such as the residue side chains of lysine and aspartic) in the iron binding (Zhang et al., 2021). The C═O absorption peak at 1655.59 cm^{-1} and the –COOH absorption peak at 1398.14 cm^{-1} showed an obvious shift after the chelation, indicating the existence of an interaction between the carboxyl group and Fe^{2+}. The amide band at 1542.77 cm^{-1}, ascribed to the N—H deformation and C—N stretching vibrations, shifted to 1551.04 cm^{-1} (Wu et al., 2021). Additionally, the absorption peak at 1089.58 cm^{-1}, associated to the-PO_3 stretching vibration, shifted to 1071.26 cm^{-1}, implying that the phosphate group was involved in the chelation. Moreover, the peak at 721.24 cm^{-1} moved to 796.45 cm^{-1}, most probably due to the vibration of the C—H and N—H bonds (Chen et al., 2013). Based upon the above data, it can be concluded that the peptides carboxyl, amino and phosphate groups might be involved in the interaction with the iron. The characterization results showed that the iron mainly chelated with carboxyl, amino and phosphate groups of peptides and the peptides stability was increased upon the chelation.

Thermal properties of the protein are commonly used to elucidate the ability to resist aggregation or denaturation during heat processing (Lan et al., 2020). As shown in Fig. 3D, a prominent double exothermic peak (123 °C) was observed for the E3 fraction; however, E3-Fe chelate showed two prominent single peaks (61 and 91 °C) with a significantly different onset temperature of denaturation. The above results indicated that the iron-chelating may be responsible for the denaturation observed in E3-Fe chelate sample, and different denaturation temperatures might be the result of the denaturation of different peptides. Compared with E3, only one broader peak with a steeper slope was observed, and it might arise from the overlapped denaturation peaks of peptides. In terms of the onset temperature, the E3-Fe fraction was characterized with a higher onset temperature, indicating increased heat stability to some extent.

3.9. Mass spectrometry of E3 fraction

The identified peptide sequences from the E3 fraction are shown in Table 2. Using LC-MS/MS, 6 peptides with a MW ranging from 1372.36 to 2937.04 Da were identified The DDSSSpSpSpSpSpSVLSK, ARIITEVNPESpEEEDE, and AGSRAAARIITEVNPESpEEEDESpSPYE were derived from phosvitin and RQSpVEDVSpSGNSF, NIRDRQSpVEDVSpSGNSF, and TDNIRDRQSpVEDVSpSGNSF were derived from vitellogenin-1. In accordance with the amino acids results shown in Table 1, the peptides were composed of 13–27 amino acid residues and exhibited common structural characteristics, such as an abundance of serine or glutamic for each peptide. Obviously, most of the serine in the identified peptides was phosphorylated. In agreement with this, numerous studies have found that hydrophilic amino acids, such as glutamic, aspartic, serine, lysine and arginine, were related to the peptide's iron-chelating ability. In detail, glutamic and aspartic increased the hydrolysate iron-chelating ability, donating free electrons in carboxyl oxygen to the iron empty orbital. Besides, the lysine ε-amino nitrogen and the arginine guanidino nitrogen might be also involved in the iron binding (Bautista et al., 1996; Kim et al., 2007). It has also been reported that serine and its phosphorylated hydroxyl group play an important role in the iron binding (Jung et al., 2006). Besides, the most abundant peptide DDSSSpSpSpSpSpSVLSK was synthesized with a purity of 98%. The iron chelating activity of the synthetic peptide was verified, the iron binding rate was 94.87 ± 1.02% and the iron ion chelating amount was 24.08 ± 1.12 mg/g.

3.10. Prediction of the mechanism of combination between *DDSSSpSpSpSpSpSVLSK* and *Fe*

According to the results of the amino acids composition, FTIR, DSC, LC-MS/MS and previous reports, it is confirmed that *DDSSSpSpSpSpSpSVLSK*-Fe is a new peptide. The possible iron binding sites are mainly involved in carboxyl, amino and phosphate groups of peptides. According to the above results, the hypothetical structure of the *DDSSSpSpSpSpSpSVLSK*-Fe was speculated in Fig. 4. Compared to other side chain groups, the phosphorylated serine residue exposure could provide more sites for binding with the iron. The interaction was combined with multiple irons, so phosphorylated serine, as a strong irons ligand, could effectively improve the iron-chelating ability.

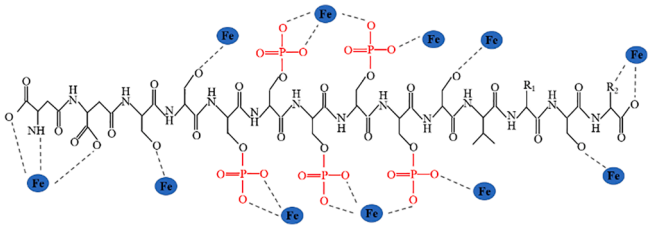

Fig. 4. The hypothetical structural of the DDSSS*S*S*S*S*SVLSK-Fe.

3.11. In vitro stability analysis of E3-Fe

The pH, temperature and digestive enzymes effects on the stability of E3-Fe complex were shown in Fig. 5. As the pH increased, the iron release rate of E3-Fe presented a general trend, firstly increasing and then remaining unchanged (Fig. 5A). In the strongly acidic conditions (pH 3), the iron release rate showed the highest value of 18.62%, suggesting that the E3-Fe structure was unstable in the strongly acidic conditions, probably due to the H^+ competing for iron with peptides and leading to the iron release from the chelate complexes (Zhang et al., 2021). The E3-Fe chelate showed very high stability under the neutral and basic conditions as the iron release rates all remained at a low value (about 7%). The iron release rate of E3-Fe at different temperatures was at a low value (about 6%) and there were no significant differences among the different groups, indicating that the E3-Fe chelate owned a high thermal stability (Fig. 5B). Fig. 5C shows the digestion stability of E3-Fe: during the 2-hours gastric digestion, the iron release rate significantly increased and reached the highest value of 21.36% at 120 min. However, the intestinal digestion resulted in an iron release rate decrease of only 11.02%. These experimental results demonstrated that E3-Fe chelate presented high overall stability in the intestinal digestion, but low stability in the gastric digestion. It might be due to the low pH value of the gastric juice which could make the E3-Fe structure unstable, as a consequence, the iron releases. Besides, another reason was that the E3-Fe would be degraded by the pepsin and the irons released from E3-Fe complex (Wu et al., 2019). However, in the pancreatic juice digestion, the environmental pH was high and the complex was more stable. Moreover, the free iron ions might be re-chelated by some small peptides decomposed under neutral and basic conditions (Udechukwu et al., 2018).

3.12. Iron transport in Caco-2 cells

Cytotoxicity tests were performed with Caco-2 cells by MTT test. The samples that decreased the absorbance at 490 nm in the MTT assay by more than 10% compared to the control were considered to be toxic. From Fig. 6A, the E3-Fe chelate showed no toxicity with a concentration of 0.25–6 mg/mL. The concentrations of 0.5, 1 and 2 mg/mL were used to study the iron transport of E3-Fe. The E3-Fe and iron sulfate samples with the same iron mass were used for the iron transport in Caco-2 cells. The iron quantity passed through the Caco-2 membrane in different groups is shown in Fig. 6B. As the iron salt concentration increased, the iron transport rate slightly increased (from 14.45 to 16.65% when the iron salt concentration increased from 20 to 80 μg/mL). In the E3-Fe

Table 2
Peptide Sequences Identified in E3 Component.

Number	Peptide sequence	MW (Da)	Relative content (%)	Organism
1	DDSSS*S*S*S*S*SVLSK	1372.36	4.55	Phosvitin
2	ARIITEVNPES*EEEDE	1859.92	1.81	Phosvitin
3	AGSRAAARIITEVNPES*EEEDES*SPYE	2937.04	1.74	Phosvitin
4	RQS*VEDVS*SGNSF	1510.58	0.04	Vitellogenin-1
5	NIRDRQS*VEDVS*SGNSF	1909.99	2.13	Vitellogenin-1
6	TDNIRDRQS*VEDVS*SGNSF	2126.18	1.09	Vitellogenin-1

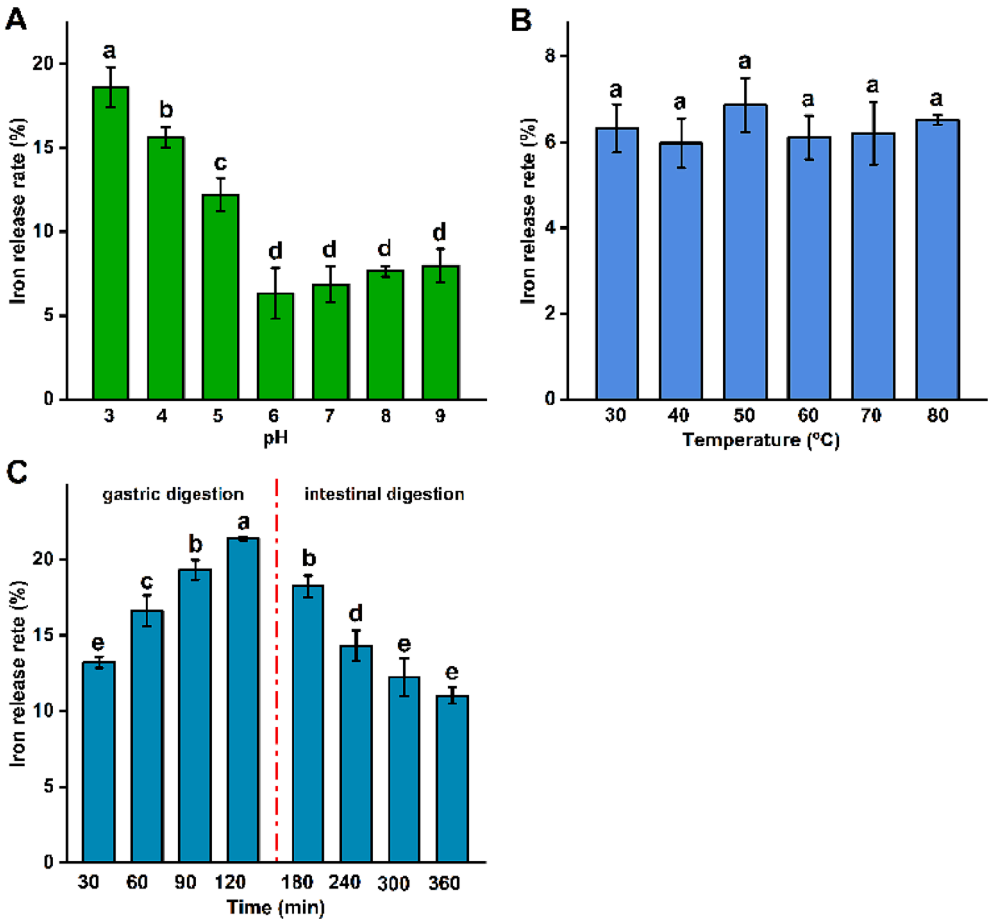

Fig. 5. The effects of the pH, temperature and digestive enzymes on the stability of E3-Fe complex: (A) iron release rate of E3-Fe under different pH values; (B) iron release rate of E3-Fe under different temperatures; (C) iron release rate of E3-Fe during gastric and intestinal digestion.

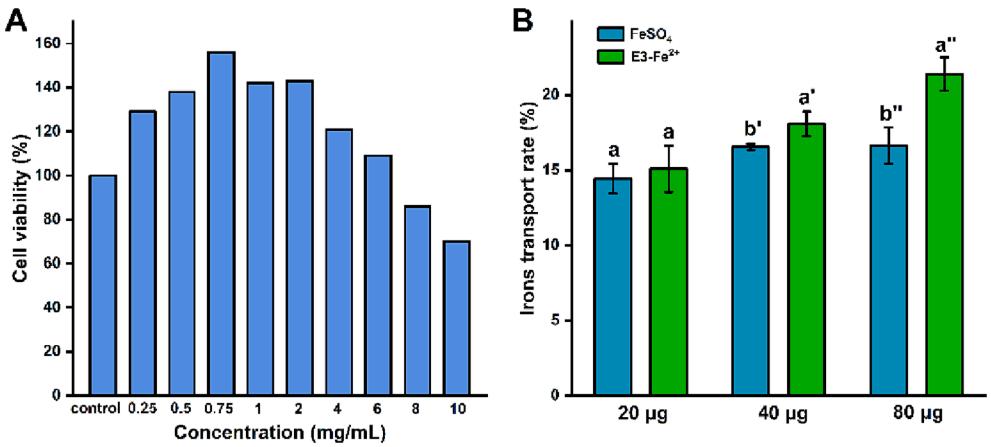

Fig. 6. In vitro evaluation of the bioavailability of E3-Fe: (A) cell viability of Caco-2 cells; (B) iron transport of E3-Fe in the Caco-2 cell membrane.

group, the irons transport rate significantly increased (from 15.10 to 21.40%) with the iron concentration increasing from 20 to 80 μg/mL. Besides, the E3-Fe groups all showed a higher iron transport rate when compared with the $FeSO_4$ groups under three different iron concentrations (20, 40 and 80 μg/mL). In other studies, some proteins and peptides reported a comparable effect such as barley iron-chelating peptides, duck egg white peptides, and whey proteins (Caetano-Silva et al., 2018; Eckert et al., 2016; Shi et al., 2021). The acquired results showed that the iron in the E3-Fe would be absorbed more effectively than the iron salts, indicating that it was possible to apply E3-Fe complex as iron supplements.

4. Conclusions

In summary, this study demonstrated that the DEYP could be used as a good source of iron-binding peptides. The hydrolysis results indicated that the selection of the enzymatic hydrolysis conditions and desirable DH was crucial in the process design and development for hydrolyzed products. This was evident in the variation in DH, MW, amino acid sequences and iron-chelating ability. The ethanol fractionation was

proved to be an effective method to accumulate iron-binding peptides. Phosphorylated serine, glutamate, carboxyl and amino in peptide chains might play a crucial role in the iron binding. The E3-Fe chelates owned a good heat, alkalinity and digestion tolerance, but a relatively bad acid tolerance. Finally, the iron in the E3-Fe would be absorbed more effectively than the iron salts. Our study provides a potential approach to prepare new iron supplements.

CRediT authorship contribution statement

Ying Liu: Conceptualization, Methodology, Software, Writing – original draft. **Zhuo Wang:** Writing – review & editing. **Abulimiti Kelimu:** Writing – review & editing. **Sameh A. Korma:** Writing – review & editing. **Ilaria Cacciotti:** Writing – review & editing. **Huan Xiang:** Writing – review & editing. **Chun Cui:** Supervision.

Declaration of Competing Interest

The authors declare that they have no known competing financial interests or personal relationships that could have appeared to influence the work reported in this paper.

Data availability

No data was used for the research described in the article.

Acknowledgments

The authors are grateful for the support by 111 Project (B17018) and the financial support from the National Natural Science Foundation of China (No. 31201416).

Appendix A. Supplementary data

Supplementary data to this article can be found online at https://doi.org/10.1016/j.fochx.2023.100692.

References

Abdul, M., Lakshmikanth, M., Lokanath, N. K., & Poornima Priyadarshini, C. G. (2022). Generation, characterization and molecular binding mechanism of novel dipeptidyl peptidase-4 inhibitory peptides from sorghum bicolor seed protein. *Food Chemistry, 369*, Article 130888.

Aluko, R. E., & Mine, Y. (1997). Competitive adsorption of hen's egg yolk granule lipoproteins and phosvitin in oil-in-water emulsions. *Journal of Agricultural and Food Chemistry, 45*(12), 4564–4570.

Aoac. (1995). *Official methods of analysis* (16th ed.). Arlington, VA, USA: Associantion of Official Analytical Chemists.

Bautista, J., Hernandez-Pinzon, I., Alaiz, M., Parrado, J., & Millan, F. (1996). Low molecular weight sunflower protein hydrolysate with low concentration in aromatic amino acids. *Journal of Agricultural and Food Chemistry, 44*(4), 967–971.

Budseekoad, S., Yupanqui, C. T., Sirinupong, N., Alashi, A. M., Aluko, R. E., & Youravong, W. (2018). Structural and functional characterization of calcium and iron-binding peptides from mung bean protein hydrolysate. *Journal of Functional Foods, 49*(333–341).

Caetano-Silva, M. E., Bertoldo-Pacheco, M. T., Paes-Leme, A. F., & Netto, F. M. (2015). Iron-binding peptides from whey protein hydrolysates: Evaluation, isolation and sequencing by LC–MS/MS. *Food Research International, 71*, 132–139.

Caetano-Silva, M. E., Cilla, A., Bertoldo-Pacheco, M. T., Netto, F. M., & Alegría, A. (2018). Evaluation of in vitro iron bioavailability in free form and as whey peptide-iron complexes. *Journal of Food Composition and Analysis, 68*, 95–100.

Cai, X., Wu, J., Tang, M., & Wang, S. (2019). Novel calcium-chelating peptides from octopus scraps and their corresponding calcium bioavailability. *Journal of the Science of Food and Agriculture, 99*(2), 536–545.

Calderón de la Barca, A. M., Ruiz-Salazar, R. A., & Jara-Marini, M. E. (2000). Enzymatic hydrolysis and synthesis of soy protein to improve its amino acid composition and functional properties. *Journal of Food Science, 65*(2), 246–253.

Chang, G.-R.-L., Tu, M.-Y., Chen, Y.-H., Chang, K.-Y., Chen, C.-F., Lai, J.-C., … Chen, C.-M. (2021). KFP-1, a novel calcium-binding peptide isolated from Kefir, promotes calcium influx through TRPV6 channels. *Molecular Nutrition & Food Research, 65*(22), 2100192.

Chen, D., Liu, Z., Huang, W., Zhao, Y., Dong, S., & Zeng, M. (2013). Purification and characterisation of a zinc-binding peptide from oyster protein hydrolysate. *Journal of Functional Foods, 5*(2), 689–697.

Dudev, T., & Lim, C. (2014). Competition among metal ions for protein binding sites: Determinants of metal ion selectivity in proteins. *Chemical Reviews, 114*, 538–556.

Eckert, E., Lu, L., Unsworth, L. D., Chen, L., Xie, J., & Xu, R. (2016). Biophysical and in vitro absorption studies of iron chelating peptide from barley proteins. *Journal of Functional Foods, 25*, 291–301.

Fang, S., Ruan, G., Hao, J., Regenstein, J. M., & Wang, F. (2020). Characterization and antioxidant properties of Manchurian walnut meal hydrolysates after calcium chelation. *LWT-Food Science and Technology, 130*, Article 109632.

Guilmineau, F., Krause, I., & Kulozik, U. (2005). Efficient analysis of egg yolk proteins and their thermal sensitivity using sodium dodecyl sulfate polyacrylamide gel electrophoresis under reducing and nonreducing conditions. *Journal of Agricultural and Food Chemistry, 53*(24), 9329–9336.

Hernández-Ledesma, B., Recio, I., Ramos, M., & Amigo, L. (2002). Preparation of ovine and caprine β-lactoglobulin hydrolysates with ACE-inhibitory activity. Identification of active peptides from caprine β-lactoglobulin hydrolysed with thermolysin. *International Dairy Journal, 12*(10), 805–812.

Huang, M., Mao, Y., Li, H., & Yang, H. (2021). Kappa-carrageenan enhances the gelation and structural changes of egg yolk via electrostatic interactions with yolk protein. *Food Chemistry, 360*, Article 129972.

Huang, X., & Ahn, D. U. (2019). How can the value and use of egg yolk be increased? *Journal of Food Science, 84*(2), 205–211.

Jantarajit, W., Thongon, N., Pandaranandaka, J., Teerapornpuntakit, J., Krishnamra, N., & Charoenphandhu, N. (2007). Prolactin-stimulated transepithelial calcium transport in duodenum and Caco-2monolayer are mediated by the phosphoinositide 3-kinase pathway. *American Journal of Physiology Endocrinology and Metabolism, 293*, E372–E384.

Jung, W.-K., Karawita, R., Heo, S.-J., Lee, B.-J., Kim, S.-K., & Jeon, Y.-J. (2006). Recovery of a novel Ca-binding peptide from Alaska Pollack (*Theragra chalcogramma*) backbone by pepsinolytic hydrolysis. *Process Biochemistry, 41*(9), 2097–2100.

Kim, S. B., Seo, I. S., Khan, M. A., Ki, K. S., Nam, M. S., & Kim, H. S. (2007). Separation of iron-binding protein from whey through enzymatic hydrolysis. *International Dairy Journal, 17*(6), 625–631.

Kong, X., Bao, S., Song, W., Hua, Y., Zhang, C., Chen, Y., & Li, X. (2021). Contributions of ethanol fractionation on the properties of vegetable protein hydrolysates and differences in the characteristics of metal (Ca, Zn, Fe)-chelating peptides. *LWT-Food Science and Technology, 146*, Article 111482.

Lan, Y., Ohm, J.-B., Chen, B., & Rao, J. (2020). Physicochemical properties and aroma profiles of flaxseed proteins extracted from whole flaxseed and flaxseed meal. *Food Hydrocolloids, 104*, Article 105731.

Liu, K., Liu, Y., & Chen, F. (2018). Effect of gamma irradiation on the physicochemical properties and nutrient contents of peanut. *LWT-Food Science and Technology, 96*, 535–542.

Liu, Q., Geng, R., Zhao, J., Chen, Q., & Kong, B. (2015). Structural and gel textural properties of soy protein isolate when subjected to extreme acid pH-shifting and mild heating processes. *Journal of Agricultural and Food Chemistry, 63*(19), 4853–4861.

Liu, Q., Kong, B., Xiong, Y. L., & Xia, X. (2010). Antioxidant activity and functional properties of porcine plasma protein hydrolysate as influenced by the degree of hydrolysis. *Food Chemistry, 118*(2), 403–410.

Mattar, G., Haddarah, A., Haddad, J., Pujola, M., & Sepulcre, F. (2022). New approaches, bioavailability and the use of chelates as a promising method for food fortification. *Food Chemistry, 373*, Article 131394.

Nisov, A., Ercili-Cura, D., & Nordlund, E. (2020). Limited hydrolysis of rice endosperm protein for improved techno-functional properties. *Food Chemistry, 302*(1), Article 125274.

O'Loughlin, I. B., Kelly, P. M., Murray, B. A., FitzGerald, R. J., & Brodkorb, A. (2015). Molecular characterization of whey protein hydrolysate fractions with ferrous chelating and enhanced iron solubility capabilities. *Journal of Agricultural and Food Chemistry, 63*(10), 2708–2714.

Peñaranda-López, A. L., Fuente, E.-B.-D., l.,, &, Torrestiana-Sánchez,, & B.. (2020). Fractionation of hydrolysates from concentrated lecithin free egg yolk protein dispersions by ultrafiltration. *Food and Bioproducts Processing, 123*, 209–216.

Shi, Q., Wei, M., Chen, H., Gao, J., & Tong, P. (2021). Desalination of duck egg white by biocoagulation to obtain peptide-ferrous chelate as iron delivery system: Preparation, characterization, and Fe^{2+} release evaluation in vitro. *Journal of Food Science, 86*(10), 4678–4690.

Shi, R., Liu, D., Sun, J., Yia, Y., & Zhang, P. (2015). Effect of replacing dietary $FeSO_4$ with equal Fe-levelled iron glycine chelate on broiler chickens. *Czech Journal of Animal Science, 60*(5), 233–239.

Sophie, W.-A., Gérard, W., Cérard, G., Andreas, B., Beat, M., Bernard, F., & Jean-Daniel, T. (2014). Physiology of iron metabolism. *Transfus. Med. Hemother., 41*, 213–221.

Steinbicker, A. U., & Muckenthaler, M. U. (2013). Out of balance-systemic iron homeostasis in iron-related disorders. *Nutrients, 5*, 3034–3061.

Sun, N., Cui, P., Jin, Z., Wu, H., Wang, Y., & Lin, S. (2017). Contributions of molecular size, charge distribution, and specific amino acids to the iron-binding capacity of sea cucumber (*Stichopus japonicus*) ovum hydrolysates. *Food Chemistry, 230*, 627–636.

Sun, S., Faza, M. A., Roy, B. C., Chandra, B., & Mallik, S. (2001). Thermodynamic studies on the recognition of flexible peptides by transition-metal complexes. *Inorganic Chemistry, 41*, 1584–1590.

Thiansilakul, Y., Benjakul, S., & Shahidi, F. (2007). Compositions, functional properties and antioxidative activity of protein hydrolysates prepared from round scad (*Decapterus maruadsi*). *Food Chemistry, 103*(4), 1385–1394.

Torres-Fuentes, C., Alaiz, M., & Vioque, J. (2012). Iron-chelating activity of chickpea protein hydrolysate peptides. *Food Chemistry, 134*(3), 1585–1588.

Udechukwu, M. C., Downey, B., & Udenigwe, C. C. (2018). Influence of structural and surface properties of whey-derived peptides on zinc-chelating capacity, and in vitro

gastric stability and bioaccessibility of the zinc-peptide complexes. *Food Chemistry, 240*, 1227–1232.

Vo, T. D. L., Pham, K. T., Le, V. M. V., Lam, H. H., Huynh, O. N., & Vo, B. C. (2020). Evaluation of iron-binding capacity, amino acid composition, functional properties of *Acetes japonicus* proteolysate and identification of iron-binding peptides. *Process Biochemistry, 91*, 374–386.

Wu, W., He, L., Liang, Y., Yue, L., Peng, W., Jin, G., & Ma, M. (2019). Preparation process optimization of pig bone collagen peptide-calcium chelate using response surface methodology and its structural characterization and stability analysis. *Food Chemistry, 284*, 80–89.

Wu, W., Jia, J., Wen, C., Yu, C., Zhao, Q., & Hu, J. (2021). Optimization of ultrasound assisted extraction of abalone viscera protein and its effect on the iron-chelating activity. *Ultrasonics Sonochemistry, 77*, Article 105670.

Xie, H., Huang, J., Woo, M. W., Hu, J., Xiong, H., & Zhao, Q. (2021). Effect of cold and hot enzyme deactivation on the structural and functional properties of rice dreg protein hydrolysates. *Food Chemistry, 345*(10), Article 128784.

Zambrowicz, A., Pokora, M., Eckert, E., Szołtysik, M., Dąbrowska, A., Chrzanowska, J., & Trziszka, T. (2012). Antioxidant and antimicrobial activity of lecithin free egg yolk protein preparation hydrolysates obtained with digestive enzymes. *Functional Foods in Health and Disease, 2*(14), 487–500.

Zhang, Y., Ding, X., & Li, M. (2021). Preparation, characterization and in vitro stability of iron-chelating peptides from mung beans. *Food Chemistry, 349*, Article 129101.

Zhao, F., Zhang, D., Li, X., & Dong, H. (2018). High-pressure homogenization pretreatment before enzymolysis of soy protein isolate: The effect of pressure level on aggregation and structural conformations of the protein. *Moleculars, 23*(7), 1775.